Disentangling the Relation Between the Planform Shape and Swimming Gait in Cetacean Propulsion

Fatma AYANCIK* and Keith W. MOORED †

Lehigh University, Bethlehem, PA, 18015, USA

Frank E. FISH‡

West Chester University, West Chester, PA, 19382, USA

Cetaceans have evolved a broad range of morphological characteristics and swimming gaits associated with enhanced thrust production, high propulsive efficiency, and reduced drag. These variations in their fluke shape and swimming gait influence their force production and energy requirements for swimming. The present study aims to disentangle the relation between the fluke shape and swimming gait in self-propelled swimming. Planform shapes are parametrized by using a NACA-inspired function where the coefficients are fit to different species of cetacea. An unsteady three-dimensional boundary element method is used to model the self-propelled flukes with a drag-producing virtual body. By interchanging the shape and gait parameters, the thrust, power, and efficiency of swimming along with the wake structures are characterized. It is determined that the shape and the gait of the fluke have a considerable influence on the wake topology and in turn the Strouhal number. The force production and power consumption of cetacean swimming is found to follow trends of lift-based propulsion with propulsive efficiencies ranging from 75–85%. It is also discovered that the effect of the shape and gait on the swimming performance are not intertwined and are in fact independent.

Nomenclature

MC	Mid-chord line distribution
C	Chord distribution
c	Chord length [m]
τ	Thickness distribution
S_w	Wetted area
C_T	Coefficient of thrust
C_P	Coefficient of power
η	Efficiency
CoT	Cost of transport
St	Strouhal number
AR	Aspect ratio

*Ph.D. Candidate, Department of Mechanical Engineering and Mechanics.
†Assistant Professor, Department of Mechanical Engineering and Mechanics.
‡Professor, Department of Biology.

I. Introduction

To generate thrust and effectively move in water, aquatic animals have evolved a wide variety of propulsive mechanisms associated with their biological role, evolutionary history, and their aquatic environment. Specifically, cetaceans such as dolphins, whales, and porpoises oscillate their moderate to high aspect ratio flukes in combined heaving and pitching motions in order to generate propulsive forces through so called lift-based mechanisms.[1] Lift-based propulsion has been shown to lead to high speed, efficiency, and maneuverability during swimming,[2–6] which has motivated numerous theoretical and numerical studies of cetacean swimming.[7–14] However, the mechanisms that lead to efficient unsteady thrust production of three-dimensional cetacean-like propulsors and the connection to its wake structure are still not well-understood.[13–16]

The early theory of lift production by a harmonically heaving and pitching two-dimensional airfoil in a potential flow was developed by Theodorsen.[18] Garrick[19] then extended this theoretical model to also determine the thrust or drag forces produced by such motions, which has led to new insights into animal swimming in recent years.[20–23,37] Similarly in the 1960s, the hydrodynamic analysis of fish and cetacean swimming was discussed by Lighthill[2] and Wu.[9,10] Their theories captured the unsteady force production of slender bodies and waving plates in a potential flow. However, many of Garrick's, Lighthill's, and Wu's theories assume that the swimming bodies or propulsors are well represented by thin profiles undergoing small amplitude motions with non-deforming, planar wakes. Following Lighthill's elongated body theory,[24] a lifting surface theory was developed[25–27] that had the same assumptions as the previous theories except it was valid for three-dimensional flows and in turn it has been used to calculate the effects of sweep on the performance of the lunate tails of fish. More recently, an asymptotic theory for three-dimensional lunate tails has been developed and is valid for high aspect ratio tails and flukes.[7] Karpouzian[7] analytically compared the performance of fins with varying aspect ratio and sweep, and both parameters were found to have a significant impact on thrust and efficiency. Also, Liu and Bose[11] applied a similar lifting surface theory to Chopra and Kambe's[27] study to examine the performance of three cetacean fluke shapes. They used a quasi-vortex-lattice numerical method. By varying pitch and heave amplitude, it was found that the tail shape significantly altered the conditions for maximum efficiency. To extend analyses beyond the limitations of these theories, boundary element methods (BEM) or panel methods were developed.

BEM solvers have been used to examine the performance of three-dimensional swimmers[12,28–31] moving at a constant velocity with non-deforming[12,28,29] and deforming wakes.[30,31] Liu & Bose[12] explored the spanwise bending of fin whale flukes and found that minimal bending led to high efficiencies greater than 80%. Cheng & Chahine[32] examined the three-dimensional wake structure produced by a swimming saithe. Zhu et al.[31] observed maximum efficiencies of 71% in tuna and giant danio both of which had high aspect ratio fins. In recent years, the boundary element method has been extended to examine the *self-propelled* swimming of bio-inspired undulatory fins[38] as well as the self-propelled performance of the manta ray.[36]

Beyond inviscid methods, Navier-Stokes solvers have also been used to examine the effects of fin shape on the flow physics and performance of swimmers. For example, Borazjani and Sotiropoulos[14] and Tytell *et al.*[13] exchanged the body shapes and swimming gaits of carangiform and anguilliform swimmers. They determined that swimmers with lunate tail shapes produced higher swimming speeds than swimmers with eel-like shapes. However, carangiform swimming gaits were more efficient at high speeds, and anguilliform gaits were more efficient at low swimming speeds. Similarly, Li *et al.* compared the effect of unforked (eel-like) plates and forked (tuna-like) plates.[16] They expressed that forked plates perform better in locomotion than unforked plates due to higher sweep angle.

However, these studies have not examined the connection between the three-dimensional shape, the unsteady gait and the performance of cetacean-like flukes during *self-propelled* swimming. Also, in many of these studies, shape and gait parameter variations are not decoupled from each other, which means that alteration of one parameter may affect the others and cause undesired performance variations. Motivated by these observations, the present study aims to determine the performance and wake structures produced by self-propelled cetacean flukes where their shape and gait are independently varied. We further address the our driving research question: in order to maximize their propulsive efficiency are cetacean fluke shapes tailored to specific swimming gaits or *vice versa*?

II. Problem Definition and Methodology

II.A. Geometry and Kinematics Definitions

There is vast inter- and intra-species fluke shape variation among cetaceans that can be quantified with the aspect ratio, sweep angle, curvature and planform area. In this study, to quantitatively characterize a fluke shape, a parametric geometry function is developed with coefficients that are fit to a given species. This function measures distances of specified locations on the flukes to define the mid-chord line and the chord distribution by using fourth and second order polynomials, respectively. The parametric geometry functions are NACA-inspired equations in that a chord distribution is wrapped around the mid-chord line just like the thickness distribution is wrapped around the camberline of NACA airfoils. The specified measurement locations are shown in figure 1 and the polynomial functions are indicated by Eq. (1) and Eq. (2). The coefficients in these equations are solved with the help of MATLAB by using the measured parameters and they can be found in table 1.

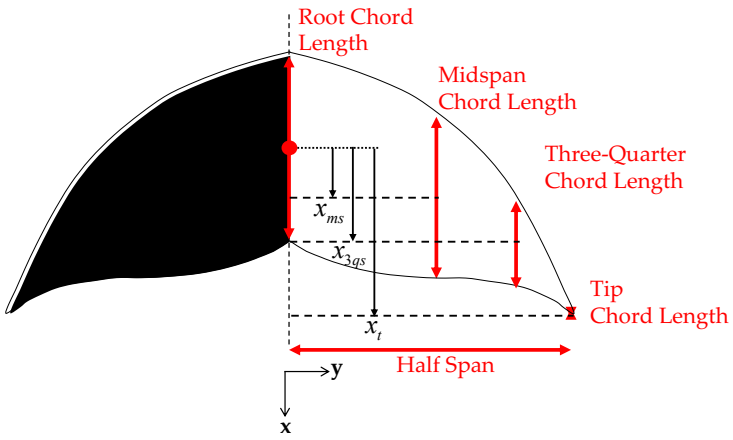

Figure 1. Demonstration of the characterization of a cetacean fluke

$$MC = A_1(y - y_0)^4 + A_2(y - y_0)^2 + A_3(y - y_0) + A_4 \tag{1}$$

$$C = F_1(y - y_0)^2 + F_2(y - y_0) + F_3 \tag{2}$$

Table 1. Coefficients of mid-chord line and chord distribution equations based on the five cetacean species.

Species Name	A1	A2	A3	A4	F1	F2	F3
Stenella plagiodon	-0.5791	0.4845	-0.4384	-0.3313	-0.7703	0.1985	0.6626
Tursiops truncatus	-0.5065	0.3549	-0.5429	-0.3838	-0.7435	-0.0356	0.7677
Delphinapterus leucas	-0.8471	1.0010	-0.8114	-0.3708	-1.2522	0.3292	0.7415
Orcinus orca	0.0172	0.0333	-0.3204	-0.3385	-0.7330	0.1297	0.6771
Pseudorca crassidens	-0.2670	0.1980	-0.3373	-0.3461	-0.3048	-0.2185	0.6923

The parametric geometry function, with its limited number of terms, provides a good approximation of the shape for various flukes. Figure 2 compares the real fluke shapes with the silhouettes of the fluke shapes obtained from the parametric function. It is noted that the approximate fluke shapes deviate from the actual flukes at the tip. However, the general fluke shape shows good agreement with the real shapes.

When the planform shape is determined based on the species, the NACA airfoil equations, Eq. (3), are then used to define the thickness distribution. In here x_c is the position along the chord where $x_c = 0$ is the leading edge and $x_c = 1$ is the trailing edge, and t_{max} is the maximum thickness as a fraction of the chord.

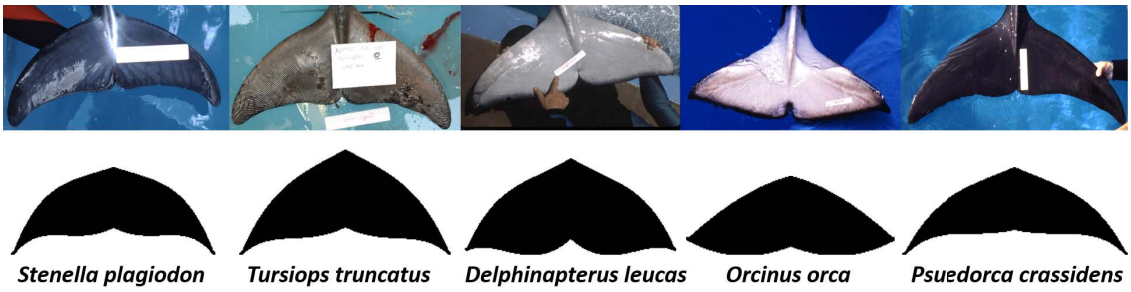

Figure 2. Real fluke images and output images of parametric geometry function

$$\tau = \frac{t_{max}}{0.2} c(0.2969\sqrt{x_c} - 0.1260x_c - 0.3516x_c^2 + 0.2843x_c^3 - 0.1015x_c^4) \tag{3}$$

To be able to isolate the planform shape effects from size scaling effects among the five species examined in this study their propulsor planform area, S_p, is kept constant by geometrically scaling the flukes such that they all have $S_p = 1$ m^2. The aspect ratio of the fluke is then defined as $AR = s^2/S_p$ where s is the scaled span length.

During self-propelled cetacean swimming, the fluke primarily produces thrust while the body primarily produces drag. In order to model the drag from the body of a cetacean and to calculate reasonable self-propelled performance metrics, a combination of a virtual body and a fluke is simulated. The virtual body is not present in the computational domain, however, a drag force is applied to the self-propelled fluke, which acts as a representation of the effect of a body. The drag from the virtual body is defined as the following,

$$D = 1/2\ C_D \rho S_w U^2, \tag{4}$$

where ρ is the density of the fluid, C_D is the coefficient of drag, S_w is the wetted surface area, and U is the time-varying swimming speed of the virtual body-fluke combination. Identical virtual body parameters are used in combination with each fluke shape in order to isolate the effects of the fluke shape and its gait on the swimming performance. In this study, $C_D = 0.01$ and $S_w = 30$ m^2, which are characteristic values for cetaceans.[39,40] In addition, the virtual body is given a mass of 263.54 to reach a self-propelled quasi-steady state quickly.

The fluke kinematics are modeled as a combined heaving and pitching motion with a fixed phase delay between pitching and heaving of $\psi = -\pi/2$,

$$\theta(t) = \theta_0 \sin(2\pi f t) \tag{5}$$

$$h(t) = h_0 \sin(2\pi f t + \psi) \tag{6}$$

Here, h_0, θ_0, and f correspond to the heave amplitude, pitch amplitude, and the oscillation frequency, respectively. A constant frequency of $f = 2$ Hz is used throughout the simulations since cetaceans swim with varying frequency on the order of $f = \mathcal{O}(1)$ Hz. All of the input parameters used in this study are listed in table 2. The heave-to-chord ratio, h_0/c, is non-dimensional amplitude of motion scaled by the root chord length, c, which can be determined from Eq. (2) when $y = y_0$ for each fluke shape.

Table 2. Shape and gait parameters of the five cetacean species

Species Name	AR	h_0/c	θ_0 [deg]	f [Hz]
Stenella plagiodon	4.50	3.75	21.53	2
Tursiops truncatus	3.90	2.51	28.85	2
Delphinapterus leucas	3.30	2.45	35.44	2
Orcinus orca	4.40	2.50	23.61	2
Pseudorca crassidens	5.60	2.85	29.03	2
Artificial gaits	3.30–5.60	2.60, 2.70, 3.30	27.00	2

II.B. Numerical Methods

An unsteady three-dimensional potential flow method is used to model the flow and to calculate the forces acting on the flukes. The flow is assumed to be irrotational, incompressible and inviscid. This reduces the governing equations to Laplace's equation $\nabla^2\Phi^* = 0$, where the perturbation potential, Φ^*, throughout the fluid is to be determined. A no-flux boundary condition is enforced on the wing surface,

$$\nabla\Phi^* \cdot \mathbf{n} = 0, \tag{7}$$

by setting the internal perturbation potential to a constant as $\Phi_i^* = 0$, that is, a Dirichlet boundary condition. The normal vector to the body's surface is $\mathbf{n}$. Also, the disturbance created by the motion should decay far from the body satisfying the far-field boundary condition.

$$\lim_{\mathbf{x}\to\infty}(\nabla\Phi^*) = 0, \tag{8}$$

where $\mathbf{x} = (x, y, z)^T$ is measured from the body-fixed frame of reference. A general solution for the internal potential at a point, P, is derived by using Laplace's equation and Green's third identity,

$$\Phi_i^*(P) = \oiint_{S_b}[\sigma(\boldsymbol{x_0})G(\boldsymbol{x};\boldsymbol{x_0}) - \mu_b(\boldsymbol{x_0})\hat{\boldsymbol{n}}\cdot\boldsymbol{\nabla}(\boldsymbol{x};\boldsymbol{x_0})]dS_0 - \oiint_{S_w}[\mu_w(\boldsymbol{x_0})\hat{\boldsymbol{n}}\cdot\boldsymbol{\nabla}(\boldsymbol{x};\boldsymbol{x_0})]dS_0, \tag{9}$$

where S_b and S_w indicate the fluke and wake surface, respectively, $\Phi_i^*(P)$ is the velocity potential of an arbitrary point within the fluke surface, and $G(\boldsymbol{x};\boldsymbol{x_0}) = -1/4\pi r$ where $r = |\boldsymbol{x} - \boldsymbol{x_0}|$. Following Katz & Plotkin's approach,[35] the solution to Laplace's equation can be obtained by distributing sources of strength σ and doublets of strength μ on the boundaries. To numerically solve the problem, a fluke is represented by a finite number N of quadrilateral constant strength elements and each element is assigned to one collocation point within the body where velocity potential set to zero to enforce the no-flux boundary condition. Then the boundary integral equation (9) with Dirichlet conditions substituted is discretized into the summation over the boundary elements as,

$$\sum_{j=1}^{N_b}(B_{ij}\sigma_j + C_{ij}\mu_j) + \sum_{k=1}^{N_w} C_{w,ik}\mu_{w,k} = 0, \tag{10}$$

$$B_{ij} = -\frac{1}{4\pi}\int_{ele}\frac{1}{|\boldsymbol{r_{ij}}|}dS_0, \tag{11}$$

$$C_{ij} = -\frac{1}{4\pi}\int_{ele}\frac{\hat{\boldsymbol{n}}\cdot\boldsymbol{r_{ij}}}{|\boldsymbol{r_{ij}}|^3}dS_0, \tag{12}$$

$$C_{w,ij} = -\frac{1}{4\pi}\int_{ele}\frac{\hat{\boldsymbol{n}}\cdot\boldsymbol{r_{ik}}}{|\boldsymbol{r_{ik}}|^3}dS_0, \tag{13}$$

$$\text{and } \boldsymbol{r_{ij}} = \boldsymbol{x_i} - \boldsymbol{x_{0,j}},\ \ \boldsymbol{r_{ik}} = \boldsymbol{x_i} - \boldsymbol{x_{0,k}}, \tag{14}$$

where N_b is the number of body elements, N_w is the number of wake elements, dS_0 is the differential area of the boundary element, $\mathbf{x_i}$ is the vector denoting the position of the i^{th} collocation point, $\mathbf{x_{0,j}}$ is the vector denoting the position of a differential area of the j^{th} element and $\mathbf{x_{0,k}}$ is the vector denoting the position of a differential area of the k^{th} element. To solve the equations, the explicit Kutta condition is enforced at the trailing edge. At each time step, a boundary element with a known doublet strength is shed from the trailing edge and the shed wake elements are advected by the local velocity. In this wake deformation process, the local velocity is calculated by using the desingularized Biot-Savart law.

After the potential field is determined, the tangential perturbation velocity over the body is found by a local differentiation of the perturbation potential. The unsteady Bernoulli equation is then used to calculate the pressure field acting on the body. The self-propelled body dynamics are calculated for one degree of freedom of translation in the streamwise direction. The body velocity and position are determined at the

current time step through forward differencing and the trapezoidal rule, respectively,

$$x_b^{n+1} = x_b^n + \frac{1}{2}(U_0^{n+1} + U_0^n)\Delta t, \tag{15}$$

$$U_0^{n+1} = U_0^n + \frac{F_x^n}{M}\Delta t. \tag{16}$$

Here F_x^n is the net force acting on the fluke in the streamwise direction at the n^{th} timestep, x_b is the body position of the fluke and Δt is the time step. Further details about unsteady boundary element method and its validation can be found in Moored.[38]

II.C. Output Parameters

The output parameters examined in this study are based on the mean values of quantities that are time-averaged over an oscillation cycle and are denoted with an overline such as $\overline{(\cdot)}$. Mean quantities are only taken after a swimmer has reached the steady-state of its cycle-averaged swimming speed. For instance, when this occurs the steady-state cycle-averaged swimming speed will be described as the mean swimming speed and denoted as $\overline{U}$. The mean swimming speed occurs when the net thrust coefficient is lower than $C_{T,net} < 10^{-5}$ where $C_{T,net} = (\overline{T} - \overline{D})/(1/2\,\rho S_p \overline{U}^2)$. Additionally, the mean swimming speed will also be reported as a nondimensional stride length,

$$U^* \equiv \frac{\overline{U}}{fL}, \tag{17}$$

which represents the distance travelled by a swimmer in body lengths over one oscillation cycle. Here, L is the body length of the swimmer, which is chosen as $L = 3$ m for all species. The reduced frequency and Strouhal number are reported as,

$$k = \frac{fc}{\overline{U}} \quad St = \frac{fA}{\overline{U}}, \tag{18}$$

where A is the peak-to-peak heave amplitude which is $A = 2h_0$. The power and thrust coefficients are normalized by added mass forces defined as,

$$C_T = \frac{\overline{T}}{\rho S_p f^2 A^2}, \quad C_P = \frac{\overline{P}}{\rho S_p f^2 A^2 \overline{U}}. \tag{19}$$

The propulsive efficiency is then the ratio of the useful power output to the power input to the fluid,

$$\eta = \frac{\overline{TU}}{\overline{P}} = \frac{C_T}{C_P}. \tag{20}$$

The cost of transport, CoT, will also be reported in this study and it represents the energy consumption per unit distance and per unit mass,

$$CoT = \frac{\overline{P}}{m\overline{U}}. \tag{21}$$

The CoT can be connected to the efficiency as $CoT = \overline{D}/m\eta$ for self-propelled swimming[41] where the time averaged thrust and drag balance each other as $\overline{T} = \overline{D}$. When CoT is rearranged based on $\overline{D}$ and η as,

$$CoT = \frac{U^{*2}}{\eta}\Big(\frac{C_D 1/2 \rho S_w L^2 f^2}{m}\Big) \tag{22}$$

II.D. Methodology

To probe the connection between the fluke shape and swimming gait during self-propelled swimming, the fluke shapes of five cetacean species and their corresponding gaits (table 2) are interchanged creating 25 shape and gait permutations. Then the thrust, power and efficiency of swimming in relation to the produced wake structures are examined. Artificial gaits that do not correspond to known species are also considered in order to more evenly resolve the parameter space. Table 2 also shows the range of artificial gait parameters used in this study.

III. Results and Discussions

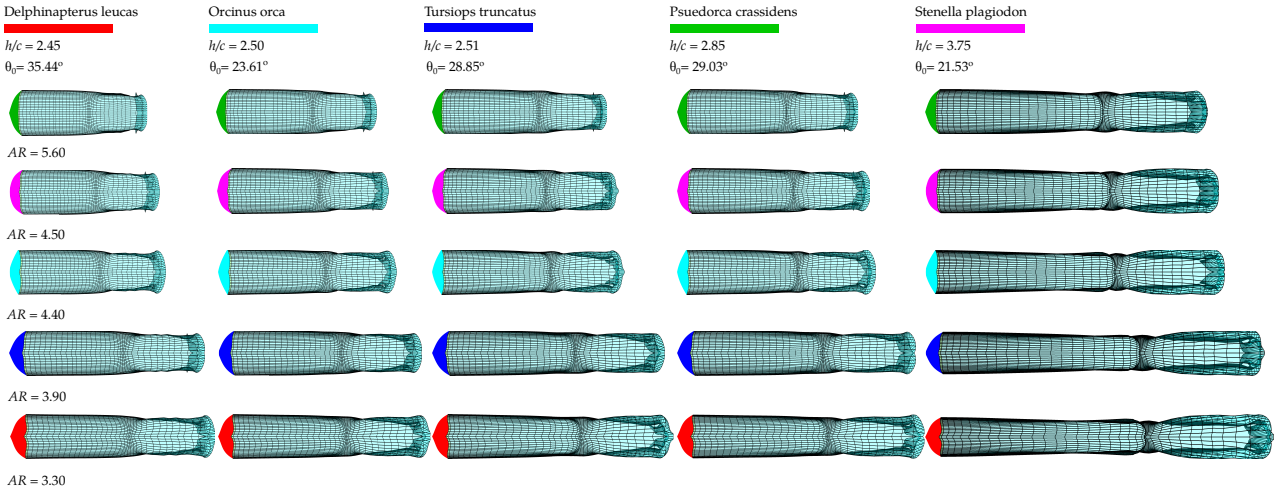

Figure 3. Compilation of wake structures. Colors represents different fluke shapes with different aspect ratio values. Wake structures are placed based on decreasing aspect ratio values from top to bottom and they are positioned based on increasing heave-to-chord-ratio from left to right.

The planform view of the element wake structures of the interchanged shape and gait cases are presented in figure 3. Each column in the wake structure image matrix corresponds to fixed gait parameters, which are indicated at the top of the column. The columns are arranged from the lowest to the highest heave-to-chord ratio going from left to right. Similarly, each row corresponds to a fixed fluke shape where the rows are arranged from the lowest to the highest aspect ratio going from bottom to top. Each species' gait parameters are indicated at the top of the figure along with the color that marks the fluke shape of the species. Figure 3 shows that self-propelled flukes shed a series of interlocking and elongated vortex ring structures, which are marked by the roll up of the wake elements. The rings take on an elliptical shape for the low-aspect-ratio flukes and a more circular shape for the high-aspect-ratio flukes. When aspect ratio is increased, the wake gets compressed in the streamwise direction relative to the span length of the fluke, yet the Strouhal number slightly decreases as indicated in figure 4. The opposite trend is observed for increasing $h/\theta_0 c$, that is, the vortex rings stretch out in the streamwise direction and since the span length is constant across a row in figure 3 then this corresponds to a drop in the Strouhal number. This trend can be seen easily in figure 4 where the Strouhal number is plotted as a function of the aspect ratio. The decrease in the Strouhal number with increasing AR and $h/\theta_0 c$ occurs due to the increased thrust production and faster swimming speeds of the high aspect ratio flukes with high amplitude motions as will be observed in the subsequent figures.

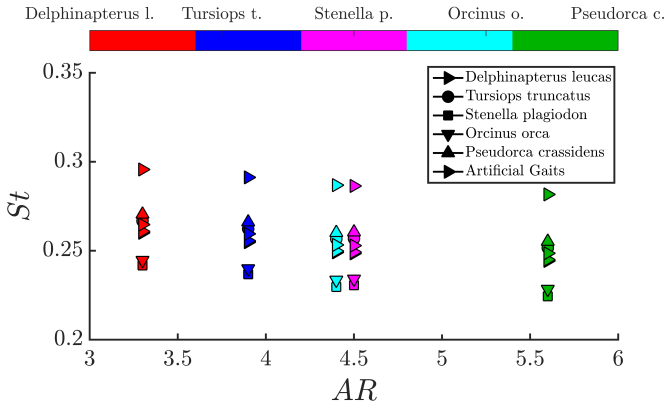

Figure 4. Strouhal number as a function of the aspect ratio. The markers denoted in the legend corresponds to the gaits of five species and artificial gaits which do not represent the gait of a particular species. The different colors denote the different fluke shapes as shown above the figure and in Figure 3.

Figure 5 shows the thrust and power coefficients as functions of the Strouhal number where the colors

and markers remain the same as the previous figures. Both the thrust and power data are predominately determined by the Strouhal number, however, the power coefficient shows a wider range of variation at a given Strouhal number. As the Strouhal number decreases, both the thrust and power increase, in general. These trends also are predicted by Garrick's theory when a harmonically heaving airfoil is modeled, but not when a harmonically pitching airfoil is modeled.[19] The distinction is that the forces for the heave case are circulatory or lift-based forces only, while for the pitch case they are dominated by added mass forces per Garrick's theory. Since the cetacean fluke thrust and power follow the trends from Garrick's heave-only case, it suggests that the force production of cetaceans is predominately circulatory or lift-based in nature.

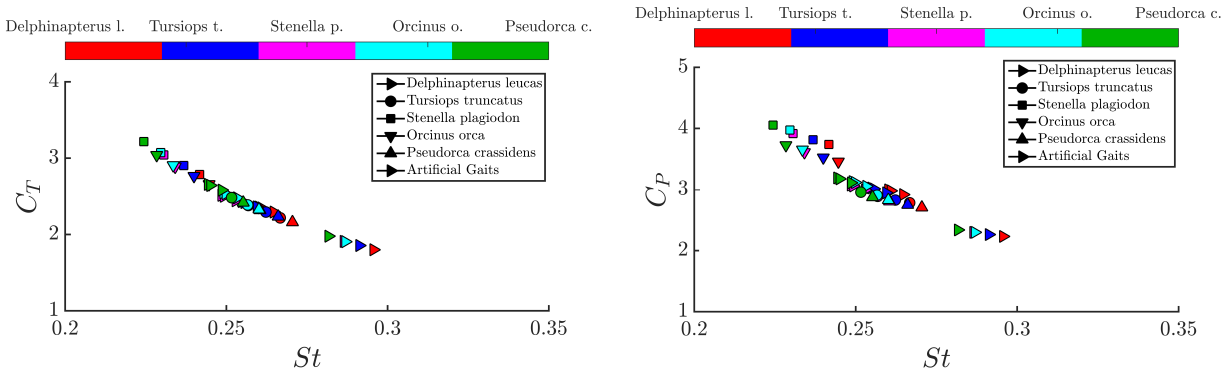

Figure 5. Self-propelled thrust and power coefficients as a function of the Strouhal number.

The propulsive efficiency η and cost of transport CoT as a function of non-dimensional stride length U^* can be seen in Figure 6. High propulsive efficiency for the cetaceans is observed in the range of 75–85%, which is in accordance with previous findings.[42] For constant gait parameters, *Pseudorca c.* shape always has the highest efficiency. Similarly, for constant shape parameters the *Delphinapterus l.* gait always has the highest efficiency. In fact, the efficiency data show that the fluke shape and its gait are *not* tailored to each other. Viewed in another way, there is one shape that maximizes the propulsive efficiency regardless of the gait and *vice versa*. The CoT is another energetic metric commonly used in biological literature since it is easier to measure than propulsive efficiency. The CoT is observed to have an increasing trend for higher values of non-dimensional stride length. At first it is surprising that all of the data collapses to a curve, however, Eq. (22) reveals the scaling trend. In Eq. (22) the parameters within the parentheses are constants for the data in this study. Consequently, the relation predicts that the CoT will vary quadratically with U^* and inversely with η, however, η varies over a small range leading to the predominant scaling with the non-dimensional stride length. In fact, the parameters for Eq. (22) are substituted along with the average efficiency of $\eta = 0.79$ and the cost of transport as a function of the non-dimensional stride length is determined and plotted in figure 6 as the dashed line. The dashed line shows good agreement with the data suggesting that it properly captures the scaling trends. Note that at the high U^* values, the CoT is under-predicted by the dashed line. This occurs since the efficiency at the high the U^* values is lower that the average of $\eta = 0.79$. The increasing trend in the CoT with non-dimensional stride length indicates that even though the efficiency is only changing slightly across the range of U^*, the amount of power expended to swim faster is increasing by a factor of 4 across the same range of U^*.

IV. Conclusions

To examine the connection between the fluke shape and the swimming gait in self-propelled cetacean swimming, the shape and gait parameters of the different species are interchanged and their performance and wake structures are investigated. When the fluke aspect ratio and heave-to-chord ratio are increased the thrust production of the cetacean is increased, consequently leading to faster swimming speeds and lower Strouhal numbers. At the same time, as the Strouhal number decreases the power coefficient is shown to increase. These trends in the thrust and power coefficients are indicative of circulatory or lift-based propulsion. It is further discovered that the effect of the shape and gait on the performance are not intertwined and are in fact independent. For instance, one shape is always more efficient than the other shapes regardless of the imposed gait and *vice versa*. Cetacean efficiencies are found to range between 75–

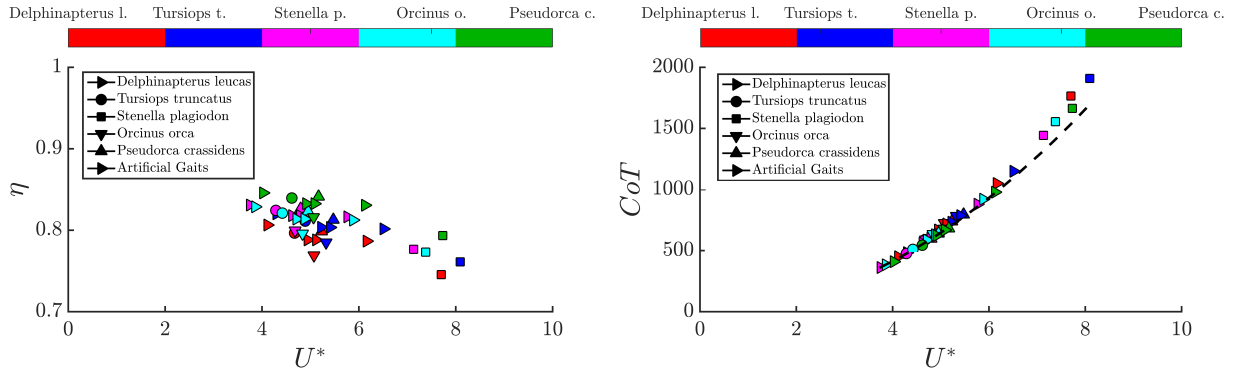

Figure 6. Self-propelled efficiency and cost of transport as a function of the non-dimensional swimming speed $U^* = U/Lf$, where L is the body length of the swimmer taken to be 3 m.

85% with the peak efficiency occurring for the *Pseudorca crassidens* shape with the *Delphinapterus leucas* gait. Finally, the cost of transport shows a quadratic trend with swimming speed as predicted by a simple scaling relation. This indicates that even though the efficiency is varying slightly over the swimming speed range, the amount of power that must be expended to swim faster is changing by up to a factor of 4.

Acknowledgments

This project is supported by the Office of Naval Research under Program Director Dr. Bob Brizzolara, MURI grant number N00014-14-1-0533.

References

[1]Fish, F.E., Rohr, J.J., (1999) Review of dolphin hydrodynamics and swimming performance. Technical Report of Space and Naval Warfare Systems Command, San Diego, California 92152-5001.

[2]Lighthill, J. 1969. Hydrodynamics of aquatic animal propulsion - a survey. Ann Rev Fluid Mech. 1:413-446.

[3]Alexander, R. McN. (1983) Animal Mechanics, 2nd Ed. Oxford: Blackwell.

[4]Daniel, T. L. 1984. Unsteady aspects of aquatic locomotion. Amer. Zool. 24: 121-134.

[5]Webb, P. W. 1988. Simple physical principles and vertebrate aquatic locomotion. Amer Zool. 28:709-725.

[6]Fish, F. E. 1996. Transitions from drag-based to lift-based propulsion in mammalian aquatic swimming. Amer. Zool. 36: 628-641.

[7]Karpouzian, G., Spedding, G. and Cheng, H. K. (1990) Lunate-tail swimming propulsion. Part 2. Performance analysis. J. Fluid Mech. 210, 329351.

[8]Cheng, H. K. and Murillo, L. E. (1984) Lunate-tail swimming propulsion as a problem of curved lifting line in unsteady flow. Part 1. Asymptotic Theory. J. Fluid Mech. 143, 327350.

[9]Wu, T. Y. (1961) Swimming of a waving plate. J. Fluid Mech. 10, 321344.

[10]Wu, T. Y. (1971) Hydromechanics of swimming propulsion. Part 1. Swimming of a two dimensional flexible plate at variable forward speeds in an inviscid fluid. J. Fluid Mech. 46, 337355.

[11]Liu, Pengfei, and N. Bose. "Propulsive performance of three naturally occurring oscillating propeller planforms." Ocean Engineering 20.1 (1993): 57-75.

[12]Liu, P., & Bose, N. (1997, August). Propulsive performance from oscillating propulsors with spanwise flexibility. In Proceedings of the Royal Society of London A: Mathematical, Physical and Engineering Sciences (Vol. 453, No. 1963, pp. 1763-1770). The Royal Society.

[13]Tytell, Eric D., et al. "Disentangling the functional roles of morphology and motion in the swimming of fish." Integrative and comparative biology (2010)

[14]Borazjani, I., & Sotiropoulos, F. (2010). On the role of form and kinematics on the hydrodynamics of self-propelled body/caudal fin swimming. Journal of Experimental Biology, 213(1), 89-107.

[15]Buchholz, J. H. J. and Smits, A. J. (2008) The wake structure and thrust performance of a rigid low-aspect-ratio pitching panel. Journal of Fluid Mechanics, Vol. 603, pp. 331-365.

[16]Li, G. J., Luodin, Z. H. U., & LU, X. Y. (2012). Numerical studies on locomotion performance of fish-like tail fins. Journal of Hydrodynamics, Ser. B, 24(4), 488-495.

[17]Borazjani, Iman, and Fotis Sotiropoulos. "Numerical investigation of the hydrodynamics of carangiform swimming in the transitional and inertial flow regimes." Journal of Experimental Biology 211.10 (2008): 1541-1558.

[18]Theodorsen, T., & Mutchler, W. H. (1935). General theory of aerodynamic instability and the mechanism of flutter.

[19]Garrick, I. E. (1937). Propulsion of a flapping and oscillating airfoil.

[20]Anderson, J. M., Streitlien, K., Barrett, D. S., & Triantafyllou, M. S. (1998). Oscillating foils of high propulsive efficiency. Journal of Fluid Mechanics, 360, 41-72. Chicago

[21]Dewey, P. A., Boschitsch, B. M., Moored, K. W., Stone, H. A., & Smits, A. J. (2013). Scaling laws for the thrust production of flexible pitching panels. Journal of Fluid Mechanics, 732, 29-46.

[22]Quinn, D. B., Moored, K. W., Dewey, P. A., & Smits, A. J. (2014). Unsteady propulsion near a solid boundary. Journal of Fluid Mechanics, 742, 152-170.

[23]Moored, K. W., & Quinn, D. B. (2017). Inviscid scaling laws of a self-propelled pitching airfoil. arXiv preprint arXiv:1703.08225.

[24]Lighthill, J., & Blake, R. (1990). Biofluiddynamics of balistiform and gymnotiform locomotion. Part 1. Biological background, and analysis by elongated-body theory. Journal of Fluid Mechanics, 212, 183-207.

[25]Cheng, J. Y., Zhuang, L. X., & Tong, B. G. (1991). Analysis of swimming three-dimensional waving plates. Journal of Fluid Mechanics, 232, 341-355.

[26]Chopra, M. G. (1976). Large amplitude lunate-tail theory of fish locomotion. Journal of Fluid Mechanics, 74(1), 161-182.

[27]Chopra, M. G., & Kambe, T. (1977). Hydromechanics of lunate-tail swimming propulsion. Part 2. Journal of Fluid Mechanics, 79(1), 49-69.

[28]Bose, N. (1995). Performance of chordwise flexible oscillating propulsors using a time-domain panel method. International shipbuilding progress, 42(432), 281-294.

[29]Liu, P. (1996). A time-domain panel method for oscillating propulsors with both chordwise and spanwise flexibility (Doctoral dissertation, Memorial University of Newfoundland).

[30]Wolfgang, M. J., Triantafyllou, M. S., & Yue, D. K. P. (1999). Visualization of complex near-body transport processes in flexible-body propulsion. Journal of visualization, 2(2), 143-151.

[31]Zhu, Q., Wolfgang, M. J., Yue, D. K. P., & Triantafyllou, M. S. (2002). Three-dimensional flow structures and vorticity control in fish-like swimming. Journal of Fluid Mechanics, 468, 1-28.

[32]Cheng, J. Y., & Chahine, G. L. (2001). Computational hydrodynamics of animal swimming: boundary element method and three-dimensional vortex wake structure. Comparative Biochemistry and Physiology Part A: Molecular & Integrative Physiology, 131(1), 51-60.

[33]Curren, Kristina C. "Designs for swimming: Morphometrics and swimming dynamics of several cetacean species." PhD diss., Memorial University of Newfoundland, 1992.

[34]Mueller, T. J. (2001). Fixed and flapping wing aerodynamics for micro air vehicle applications (Vol. 195). AIAA.

[35]Katz, J., & Plotkin, A. (2001). Low-speed aerodynamics (Vol. 13). Cambridge university press.

[36]Fish, F. E., Schreiber, C. M., Moored, K. W., Liu, G., Dong, H., & Bart-Smith, H. (2016). Hydrodynamic performance of aquatic flapping: efficiency of underwater flight in the manta. Aerospace, 3(3), 20.

[37]Akoz, E., & Moored, K. W. (2018). Unsteady propulsion by an intermittent swimming gait. Journal of Fluid Mechanics, 834, 149-172.

[38]Moored, K.W. (2018). Unsteady three-dimensional boundary element method for self-propelled bio-inspired locomotion. Computers & Fluids, 167, 324-340.

[39]Fish, F. E. (1993). Power output and propulsive efficiency of swimming bottlenose dolphins (Tursiops truncatus). Journal of Experimental Biology, 185(1), 179-193.

[40]Fish, F. E. (1998). Comparative kinematics and hydrodynamics of odontocete cetaceans: morphological and ecological correlates with swimming performance. Journal of Experimental Biology, 201(20), 2867-2877.

[41]Fish, F. E., Kolpas, A., Crossett, A., Dudas, M. A., Moored, K. W., & Bart-Smith, H. (2018). Kinematics of swimming of the manta ray: three-dimensional analysis of open-water maneuverability. Journal of Experimental Biology, 221(6), jeb166041.

[42]Fish, F. E., & Lauder, G. V. (2006). Passive and active flow control by swimming fishes and mammals. Annu. Rev. Fluid Mech., 38, 193-224.